
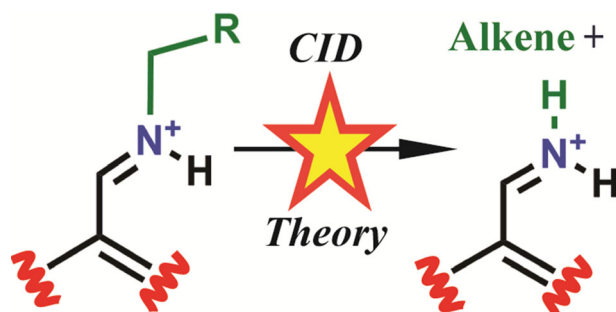


Leaving Group Effects in a Series of Electrosprayed $C_cH_hN_1$ Anthracene Derivatives

Maha T. Abutokaikah, Giri R. Gnawali, Joseph W. Frye, Curtis M. Stump, John Tschampel, Matthew J. Murphy, Eli S. Lachance, Shanshan Guan, Christopher D. Spilling, Benjamin J. Bythell 

Department of Chemistry and Biochemistry, University of Missouri, St. Louis, MO 63121, USA



Abstract. We investigate the gas-phase structures and fragmentation pathways of model compounds of anthracene derivatives of the general formula $C_cH_hN_1$ utilizing tandem mass spectrometry and computational methods. We vary the substituent alkyl chain length, composition, and degree of branching. We find substantial experimental and theoretical differences between the linear and branched congeners in terms of fragmentation thresholds, available pathways, and

distribution of products. Our calculations predict that the linear substituents initially isomerize to form lower energy branched isomers prior to loss of the alkyl substituents as alkenes. The rate-determining chemistry underlying these related processes is dominated by the ability to stabilize the alkene loss transition structures. This task is more effectively undertaken by branched substituents. Consequently, analyte lability systematically increased with degree of branching (linear < secondary < tertiary). The resulting anthracen-9-ylmethaniminium ion generated from these alkene loss reactions undergoes rate-limiting proton transfer to enable expulsion of either hydrogen cyanide or CNH. The combination of the differences in primary fragmentation thresholds and degree of radical-based fragmentation processes provide a potential means of distinguishing compounds that contain branched alkyl chain substituents from those with linear ones.

Keywords: Gas-phase structure, Imine, Density functional theory, CID, Petroleum, Oil, Protonation

Received: 28 April 2019/Revised: 18 July 2019/Accepted: 18 July 2019/Published Online: 10 August 2019

Introduction

Chemical structure determines the behavior and function of a compound, which in turn informs use and processing. A single stage of high-resolution and high mass accuracy mass spectrometry [1–6] enables confident characterization of the elemental compositions present (with uncertainties) [7], but not the specific structures. The confidence in these assignments is finite and varies based on instrument type, experimental

approach, and individual sample [7]. Consequently, tandem mass spectrometry (MS/MS) [8] is subsequently employed to isolate a single component of the sample, which is then activated and fragmented into ideally diagnostic charged pieces which are detected. Based on the mass-to-charge ratios (m/z) of the detected charged fragments, the precursor ion, and any other known chemical information or evidence, structural assignments are inferred [7, 9].

The simplest means of interpretation of tandem mass spectra is direct comparison with spectra of known standards collected under the same experimental conditions [10, 11]. For many important classes of chemicals, libraries are currently either unavailable or are limited by the impracticality of synthesizing the enormous number of possibilities necessary. Consequently, other algorithmic approaches have been developed as

Electronic supplementary material The online version of this article (<https://doi.org/10.1007/s13361-019-02298-0>) contains supplementary material, which is available to authorized users.

Correspondence to: Benjamin Bythell; e-mail: bythellb@umsl.edu

alternative methods to identify some of these chemicals [12–17]. How effective these approaches are is a function of the general quality of the models utilized, which in turn is a function of the level of (sometimes indirect) knowledge of what the dissociation chemistries at play produce and the amount and breadth of data available for comparison [7]. Consequently, our ability to confidently identify a particular analyte is inherently biased by what has gone before; meaning that as a field, mass spectrometric structural identification methods are generally much more effective at identifying materials in areas in which substantial experimental and informatics work has previously occurred.

For example, in areas such as the study of protonated species such as oils/petroleum [2, 3, 18–33], weathered [34–37], or partially decayed organic materials [38–41], or even synthetic degradation of large polyaromatic hydrocarbon materials [42], tandem mass spectral libraries are limited or non-existent and there are far too many potential chemicals for widespread synthesis of standards to be practical. Researchers would benefit from additional, complementary algorithmic and experimental methods to aid compound identifications. At present, much of the literature on fundamentals is concerned with IR spectroscopy and/or statistical modeling of radical cation analytes [43–51], or fixed charge “thermometer” ions [52–62], rather than protonated ones. However, recent work from the Vala Group examined protonated 1,2,3,4-tetrahydronaphthalene with detailed electronic structure calculations of the many isomerization pathways on the way to fragmentation of this cation [63]. The authors spectroscopically characterized the precursor ions providing evidence for population of two sites of protonation. Additional theoretical evidence of feasible formation of a benzylium ion and the classically invoked tropylium $C_7H_7^+$ structure via a series of 1,2-H-shifts was provided from density functional calculations. Differential mobility data from the Campbell and Hopkins groups [64] provided evidence of differing tautomeric populations of protonated aniline as a function of conditions. These populations in turn produced differing abundances for fragment ions. Tandem mass spectrometry of larger protonated or radical cation analytes which include one or more alkyl substituents is commonly applied [18, 19, 32, 34, 46, 47, 65, 66]. Typically, these studies are concerned with identifying broad information on complex samples rather than specifics on individual structures. Consequently, many of these spectra are from mixtures of precursor ions, so the provenance of “individual” fragment peaks is obscured. A better understanding of which protonated precursors generated which fragments and the energetic dependence of these processes would lead to more detailed and thus effective characterization.

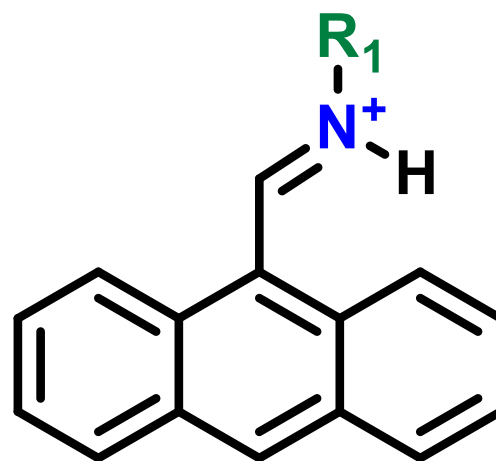
One approach to improving our understanding of a chemical class is systematic generation of model compounds which can then be analyzed with high-resolution tandem mass spectrometry experiments. Simultaneously, electronic structure calculations can be utilized to help elucidate the key diagnostic

fragmentation chemistries at play and provide evidence in support of fragment identities [65, 66]. The present article describes our targeted approach concerned with a class of derivatized polyaromatic hydrocarbon analytes with the formula $C_cH_hN_1$ (Scheme 1) analyzed by electrospray ionization MS/MS and theory. Anthracene in addition to being a crude oil component [2, 3, 18–31, 33] has been implicated in fields as wide ranging as environmental chemistry [67–70] and astrochemistry [43, 44, 71]. Here, we investigate protonated imine anthracene derivatives. The formation of protonated imines in the gas-phase has been studied as a mechanistic tool [72, 73], and as part of peptide fragmentation chemistry (a_n ion chemistry) with theory and multiple types of experimental approach [74–82]. Such analyses of protonated imine precursors have yet to be performed. Here, we address this gap by systematically altering the substituent’s (Scheme 1) chain length and degree of branching to gain insight into the affect this has on the gas-phase ions in terms of stability, dissociation mechanism, and energetics. This knowledge of leaving-group effects [83, 84] provides a direct means of chemical classification for this class of analyte which complements earlier work on related systems [19, 32, 46, 47, 65, 66, 85]. The present, initial data are part of a much wider study; the results of which will be communicated in due course.

Experimental Methods

The acetonitrile, 9-anthracenecarboxaldehyde, amines, formic acid, and deuterated methanol (CH_3OD) were purchased from Sigma-Aldrich Chemical Company (St. Louis, USA). The anthracene derivatives (Scheme 1) were synthesized based on published experimental procedures [86, 87]; details of which are provided in the supporting information.

Tandem mass spectrometric work was carried out using a MaXis plus quadrupole (hQh) electrospray time-of-flight mass spectrometer (Bruker, Billerica, MA). The instrument



Scheme 1. Generic protonated imine model compound, $[C_cH_hN_1+H]^+$, investigated in this study. R_1 is a linear (C_4H_9 , C_5H_{11} , C_6H_{13} , and C_7H_{15}) or branched alkyl group (cyclohexane or tertiary-butyl)

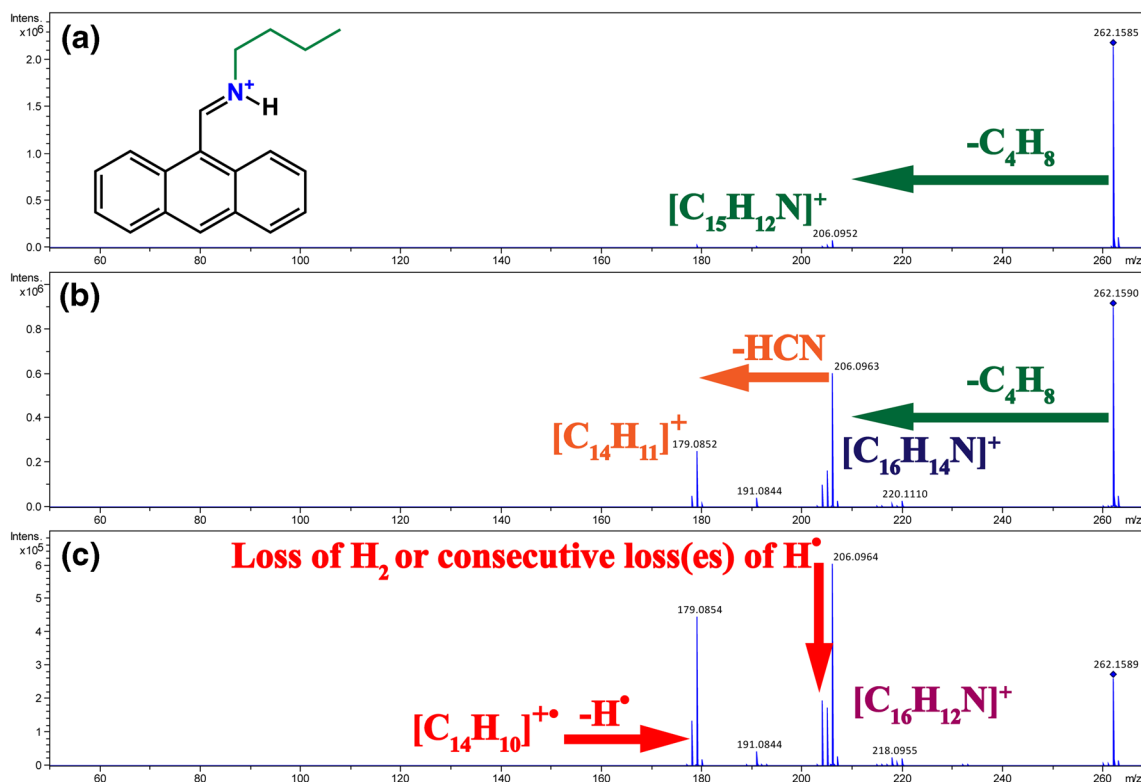


Figure 1. Example of MS/MS spectra of C_4H_9 alkyl chain substituent, $[C_{19}H_{20}N]^+$, m/z 262, at different laboratory collision energies, (a) 15 eV, (b) 25 eV, (c) 30 eV, respectively

configuration has a hexapole then quadrupole followed by an enclosed hexapole collision cell pressurized with dry nitrogen ($\sim 10^{-2}$ mbar). Conditions are such that analyte ions experience multiple collisions in each experiment. MS/MS spectra were obtained by quadrupole isolation of the precursor ion followed by collision-induced-dissociation (CID) in the collision cell, then product ion dispersion by the time-of-flight analyzer. For further analysis, pseudo-MS³ experiments were performed for specific fragment ions (m/z 206, and m/z 179). In this approach, the desired ions are generated in the source by adjusting the potential difference between the two ion funnels located at the front of the instrument. The fragment ions are then isolated in the quadrupole for CID followed by mass analysis.

Ionization was by electrospray with the samples infused into the instrument in ~ 5 μ M acetonitrile (100/0.1% formic acid)

solutions at a flow rate of 3 μ l min^{-1} . For comparison with the protonated analyte, $[M+H]^+$, data, $[M+D]^+$ cations were generated by diluting each analyte in acetonitrile/ CH_3OD (50/50%) to a final concentration of ~ 5 μ M, prior to electrospray ionization. Data were collected as a function of collision energy. Break-down graphs expressing the relative fragment ion signals as a function of collision energy were obtained for all protonated analytes. Sixty spectra were averaged for each data point. Nitrogen was used as nebulizing, drying, and collision gas.

Theoretical Methods

Simulations were performed using density functional theory. Geometry optimizations of multiple candidate

Table 1. Experimental and Theoretical Thresholds of the Precursor Ions (Anthracene Ring Substituents Listed in This Study)

Substituent	Experimental onset (E_{coll}) (eV)	Theoretical onset (kJ mol^{-1})	$E_{50\%}$	DOF	$E_{50\%}/\text{DOF}$
C_4H_9	15	270	26.8	114	23.5
C_5H_{11}	15	265	29.9	123	24.1
C_6H_{13}	15	263	30.5	132	23.1
C_7H_{15}	15	266	31.9	141	22.6
Cyclohexane	5	234	24.0	126	19.0
Tertiary-butyl	5	199	15.4	114	13.5

Collision energies at 50% precursor ions survival (m/z) $E_{50\%}$, and the degree of freedom (DOF) values are listed. $E_{50\%}/\text{DOF}$ is 50% precursor ions survival $E_{50\%}$ divided by the DOF, normalized by multiplication by a factor of 100

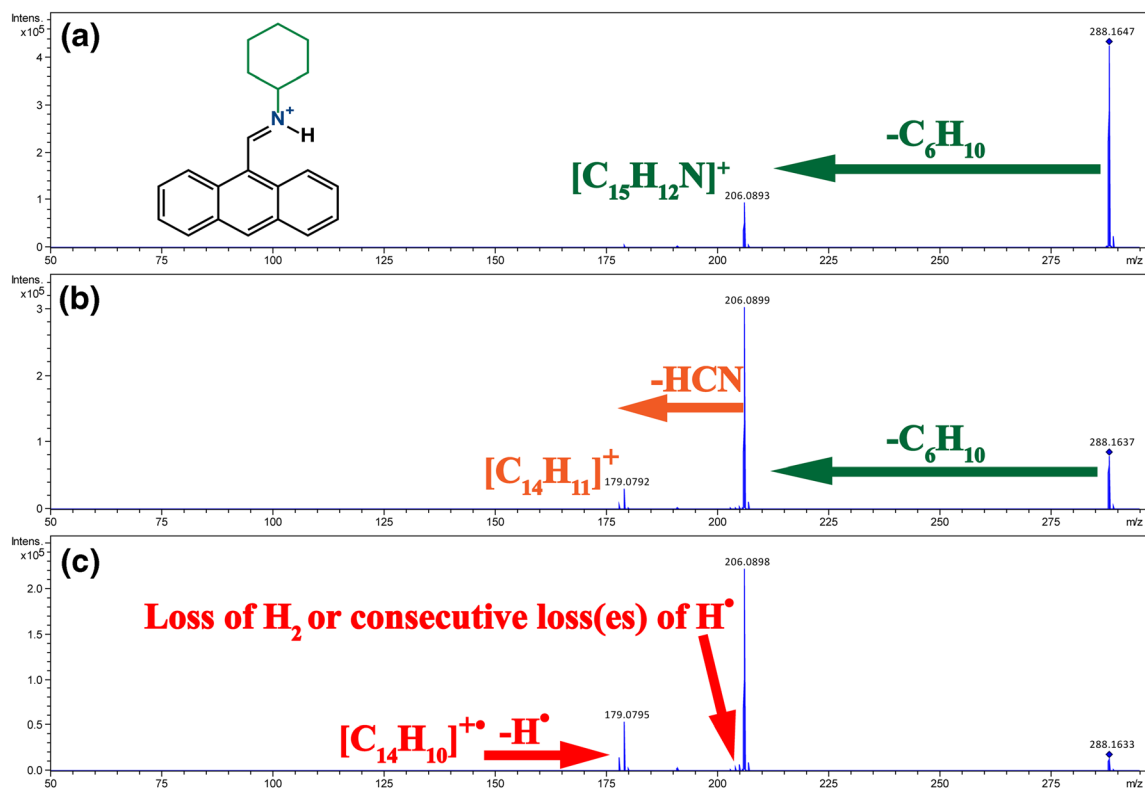


Figure 2. Example of MS/MS spectra of cyclohexane substituent $[C_{21}H_{22}N]^+$, m/z 288, at different laboratory collision energies, (a) 15 eV, (b) 25 eV, (c) 30 eV, respectively

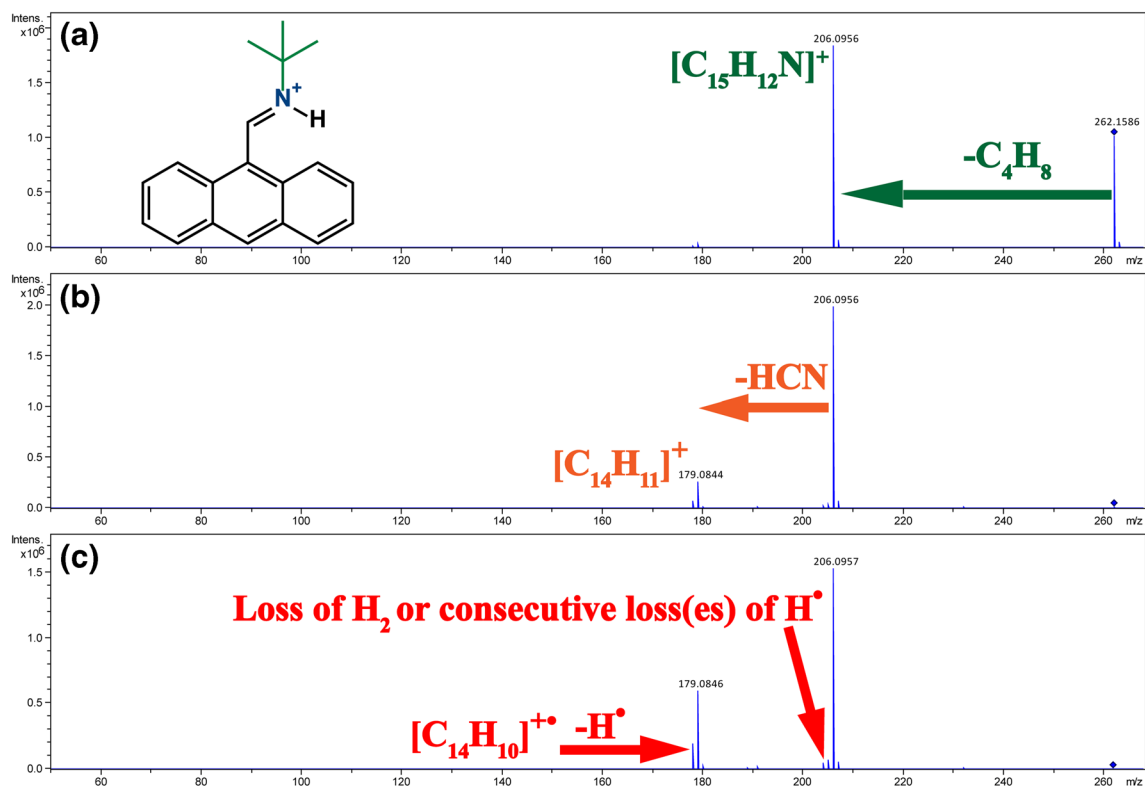
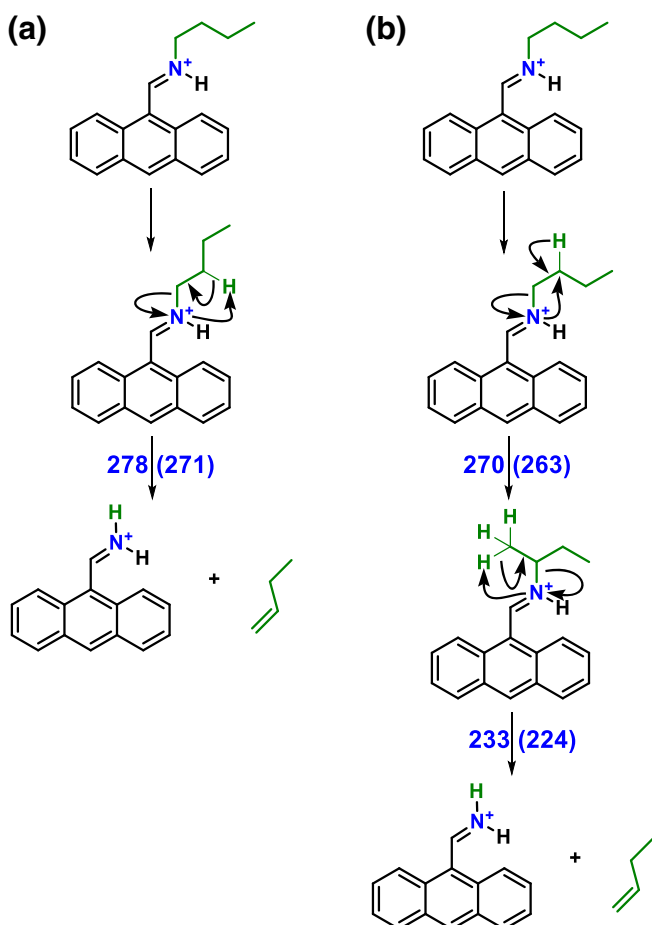


Figure 3. Example of MS/MS spectra of tertiary butyl $[C_{19}H_{20}N]^+$, m/z 262, at different laboratory collision energies, (a) 15 eV, (b) 25 eV, (c) 30 eV, respectively



Scheme 2. Lowest energy mechanisms of but-1-ene loss illustrated for the analyte with $R_1 = C_4H_9$. **(a)** Direct C–N bond cleavage of the alkyl chain to form $C_{15}H_{12}N^+$, m/z 206; **(b)** isomerization of the alkyl chain, followed by C–N bond cleavage. The relative energies ($\Delta E_{el+ZPE,0K}$ (ΔG_{298K}) in kJ mol^{-1}) of the transition structures calculated at the M06-2X/6-311G(2d,2p) level of theory are provided for illustration

conformations were performed with the Gaussian 09 software [88] package culminating in calculations at the M06-2X/6-311G(2d,2p) [89] level of theory. The minima, transition structures, and separated products of these analytes were characterized. Initial explorative investigations were performed at the M06-2X/6-311G(d) level of theory. Multiple transition structures (TSs) were calculated for each potential fragmentation pathway. Minima and TSs were tested by vibrational analysis (all real frequencies or 1 imaginary frequency, respectively). The potential energy surface generated combined the zero-point energy (ZPE) correction to the electronic energy (E_{el} , 0 K) for improved accuracy ($\Delta E_{el+ZPE,0K}$). The related, standard enthalpy (ΔH_{298K}), Gibbs free energy (ΔG_{298K}), and entropy (ΔS_{298K}) corrections to 298 K were also determined. The reaction pathway through each TS was determined by intrinsic reaction coordinate (IRC) calculations with up to eight steps in each direction. The

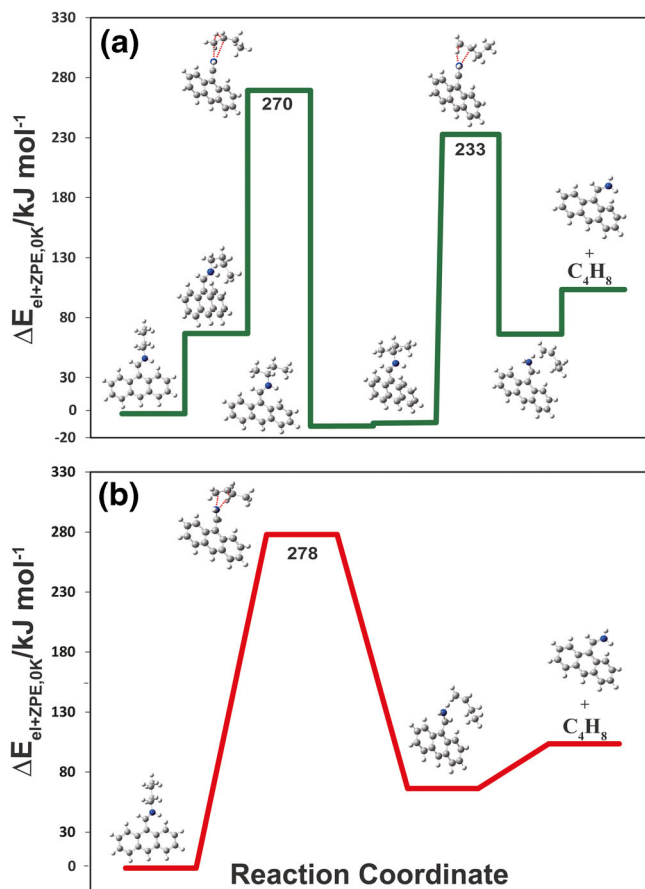


Figure 4. Minimum energy reaction pathway of the competing alkene loss pathways (but-1-ene loss) from the C_4H_9 alkyl chain substituent $[C_{19}H_{20}N]^+$. **(a)** Lowest energy pathway of alkene loss in which the alkyl chain is isomerized to a branched butyl substituent, followed by C–N bond cleavage and the product ion of the anthracen-9-ylmethaniminium product ion. **(b)** Competing, higher energy, direct loss of but-1-ene to form the same product ion. Values of the rate-determining TSs are provided for clarity (kJ mol^{-1}).

terminating points of these calculations (one on product-side, one on reactant-side) were then optimized at the same level of theory to determine which minima were connected to each TS.

Results and Discussion

Scheme 1 shows the family of anthracene-derivatized imine analytes investigated here. We systematically varied the alkyl chain length to enable an assessment of substituent size effects on the protonated imine analytes MS/MS spectra. We then addressed whether the degree of branching in the alkyl substituent has a noticeable effect on the MS/MS spectra with secondary and tertiary alkyl substituents.

Table 2. Relative Energies of the Minima, Transition Structures, and Separated Products of Alkyl Chain C_4H_9 , Substituent Calculated at the M06-2X/6-311G(2d,2p) Level of Theory

Minima and TSs	E_{el}/H	E_{el+ZPE}/H	$\Delta E_{el+ZPE,0K}/kJ\ mol^{-1}$	$\Delta H_{298}/kJ\ mol^{-1}$	$\Delta G_{298}/kJ\ mol^{-1}$	$\Delta S_{298}/J\ K^{-1}\ mol^{-1}$
GM (singlet state)	-790.486338	-790.140382	0	0	0	0
Lowest energy triplet	-790.427133	-790.083676	148.9	149.8	147.0	9.6
Alkyl chain isomerization TS1	-790.375062	-790.037707	269.6	272.9	262.7	34.7
Post-isomerization alkene loss TS2	-790.388887	-790.051707	232.8	236.3	224.3	41.0
Direct loss TS	-790.371913	-790.034358	278.4	281.0	270.6	35.6
$C_4H_9^+$ loss TS	-790.343336	-790.005480	354.2	356.5	348.2	28.4
Consecutive forming of m/z 205 TS	-790.275306	-789.947931	505.3	509.8	448.5	209.0
27 u loss proton transfer TS	-790.348308	-790.015414	328.1	329.8	278.7	174.4
Trans-cis rotation TS	-790.362626	-790.028434	293.9	297.3	241.2	190.9
HCN loss TS	-790.360117	-790.028548	293.6	297.1	243.1	183.7
Products ions and neutrals	E_{el}/H	E_{el+ZPE}/H	$\Delta E_{el+ZPE,0K}/kJ\ mol^{-1}$	$\Delta H_{298}/kJ\ mol^{-1}$	$\Delta G_{298}/kJ\ mol^{-1}$	$\Delta S_{298}/J\ K^{-1}\ mol^{-1}$
$[C_{15}H_{12}N]^+ + C_4H_8$	-790.441928	-790.100952	103.5	103.6	53.5	171.0
$[C_{15}H_{11}N]^+ + C_4H_9^{\bullet}$	-790.341831	-790.007560	348.7	353.8	292.1	210.2
$[C_{15}H_{11}N]^+ + H^{\bullet} + C_4H_8$	-790.281558	-789.955295	485.9	494.2	406.2	299.9
$[C_{14}H_{11}]^+ + HCN + C_4H_8$	-790.386571	-790.053948	226.9	233.2	132.3	343.8
$[C_{14}H_{11}]^+ + CNH + C_4H_8$	-790.348791	-790.017682	323.1	329.5	227.2	348.6

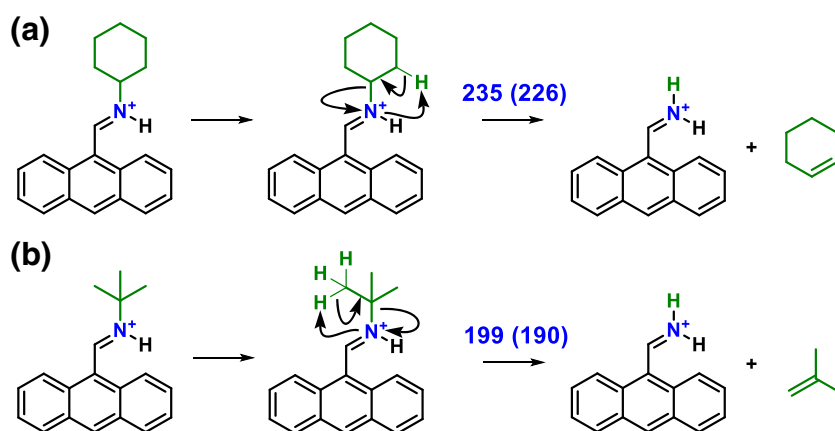
GM is the global minimum of the potential energy surface of the alkyl chain C_4H_9 substituent. Direct loss TS is the direct loss of the alkene transition state with no isomerization that includes H transfers from 2C-1C

Tandem Mass Spectra

All precursor ions with linear alkyl substituents initially produced a substantial peak at m/z 206 $[C_{15}H_{12}N]^+$ (Figure 1) that corresponds to loss of an alkene with concomitant transfer of a proton. We found that the series of precursor ions with linear alkyl substituents all behaved similarly, producing onsets of fragmentation at ~ 15 eV (laboratory collision energy). Comparisons made at the collision energies necessary to achieve 50% dissociation of the precursor peak ($E_{50\%}$, Table 1) suggest a small increase in $E_{50\%}$ with alkyl chain length. However, crude normalization of this value for the systematic change in the ($3 \times$ number of atoms - 6) degrees of freedom ($E_{50\%}/DOF$) produced similar values with alkyl chain length. At higher collision energies, the following general observations can be made: (1) consecutive loss of 27 u (HCN or CNH) generates the abundant peak at m/z 179,

$[C_{14}H_{11}]^+$; (2) radical cations are increasingly prevalent (m/z 205 and 178) resulting from either consecutive loss of hydrogen radicals or higher energy, radical-based fragmentations of the precursor ion; (3) production of more highly conjugated species occurs via additional losses of hydrogen radicals or hydrogen molecules and (4) the extent of the latter two radical-based processes was reduced as the alkyl side chain length increased (data not shown).

The branched precursor ions (cyclohexyl and tertiary-butyl) are substantially more labile than the linear alkyl imine substituted precursor ions (Figures 2 and 3; Table 1). The trend in ease of fragmentation is thus linear < secondary < tertiary alkyl substituent (Table 1; Figures 1, 2, and 3), i.e., the opposite of the $E_{50\%}$ values. The abundant alkene loss from the imine nitrogen substituent followed by consecutive loss of 27 u is consistent with the preceding linear congeners. However, the degree of radical-based direct and/or consecutive processes are



Scheme 3. (a) Mechanism of loss of cyclohexene illustrated for the analyte with $R_1 =$ cyclohexane, C_6H_{11} . Direct C–N bond cleavage produces $C_{15}H_{12}N^+$, m/z 206. (b) Mechanism of loss of 2-methylprop-1-ene by direct C–N bond cleavage to produce $C_{15}H_{12}N^+$, m/z 206. The relative energy ($\Delta E_{el+ZPE,0K}$ (ΔG_{298K}) in $kJ\ mol^{-1}$) of the transition structure calculated at the M06-2X/6-311G(2d,2p) level of theory is provided for illustration

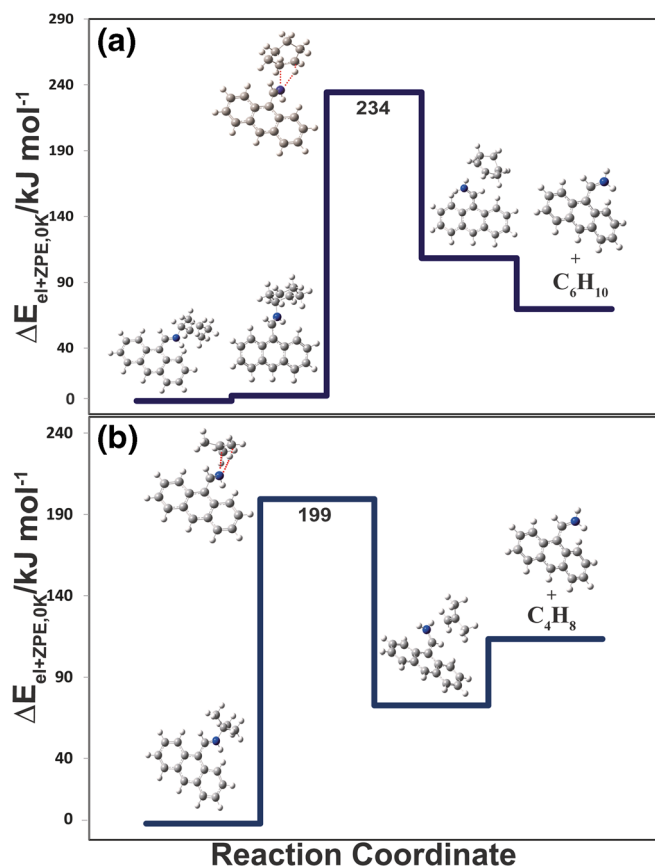


Figure 5. Minimum energy reaction pathway plots for loss of the respective alkenes from the branched substituents. (a) Cyclohexene loss from the cyclohexane substituent of $[C_{21}H_{22}N]^+$, $R_1 = C_6H_{11}$. (b) Loss of 2-methylprop-1-ene from the tertiary-butyl substituent of $[C_{19}H_{20}N]^+$, $R_1 = C_4H_9$. Values of the rate-determining TSs are provided for clarity (kJ mol^{-1})

greatly reduced for the branched precursor ions. These results provide a potential means of distinguishing compounds that contain branched alkyl chain substituents from those with linear ones.

We also performed parallel experiments with deuterated precursor ions, $[M+D]^+$. These data (Figures S1–S3) show a systematic shift of 1 u in both the precursor ions and the major dissociation pathway product peaks ($m/z 206 \rightarrow m/z 207$ and $m/z 179 \rightarrow m/z 180$). Consequently, these products all contain a single deuterium which any subsequent mechanistic proposals will need to account for. This simple labeling experiment shows (1) that the initial loss of alkene is solely from the substituent R_1 and (2) that the subsequent loss of 27 u does not include the ionizing proton (deuteron). Additionally, these analytes showed highly similar dependencies on collision energy to the protonated congeners.

Pseudo-MS³ Mass Spectra

We took pseudo-MS³ mass spectra from each of the analytes to provide an assessment of whether our consecutive fragmentation and common fragment hypotheses were plausible. Following dissociation of each protonated precursor in the source, we successively isolated the $m/z 206$ and $m/z 179$ peaks and collisionally activated them. The resulting pseudo-MS³ spectra of the $m/z 206$ population primarily produced the $m/z 179$ and 178 peaks in extremely similar abundances in all cases (Figure S4). Consistent with this finding, the pseudo-MS³ spectra of the $m/z 179$ population overwhelmingly produced the $m/z 178$ peak (loss of $H\cdot$) followed by a low abundance $m/z 152$ peak (subsequent loss of $C_2H_3\cdot$) at higher collision energies (Figure S5). Again, the data were extremely similar for each of the six analytes.

Mechanisms of Loss of the Alkyl Substituents

We performed multiple series of calculations in order to identify the precursor ion minima and major fragmentation pathways of each of the analytes. Experimentally, the most facile degradation pathway was loss of the alkyl substituent as an alkene to produce the anthracen-9-ylmethaniminium peak at $m/z 206$. For the linear alkyl chains, this reaction could in principle proceed directly (Scheme 2a) or via a more complex

Table 3. Relative Energies of the Minima, Transition Structures, and Separated Products of Branched C_6H_{11} Substituent (Cyclohexane), $[C_{21}H_{22}N]^+$, Calculated at the M06-2X/6-311G(2d,2p) Level of Theory

Minima and TSs	E_{el}/H	E_{el+ZPE}/H	$\Delta E_{el+ZPE,0K}/\text{kJ mol}^{-1}$	$\Delta H_{298}/\text{kJ mol}^{-1}$	$\Delta G_{298}/\text{kJ mol}^{-1}$	$\Delta S_{298}/\text{J K}^{-1} \text{mol}^{-1}$
GM (singlet)	-867.907197	-867.52326	0	0	0	0
Lowest energy triplet	-867.849652	-867.468709	143.2	143.9	139.7	14.4
Cyclohexane loss TS	-867.809051	-867.433941	234.5	238.2	226.3	40.6
$C_6H_{11}\cdot$ loss TS	-867.767521	-867.39212	344.4	346.7	338.2	29.1
Consecutive forming of $m/z 205$ TS	-867.693906	-867.328352	511.7	516.2	450.9	222.6
27 u loss proton transfer TS	-867.766908	-867.395835	334.6	336.2	281.0	188.0
Trans-cis rotation TS	-867.781226	-867.408855	300.4	303.6	243.6	204.5
HCN loss TS	-867.778717	-867.408969	300.1	303.4	245.5	197.3
Products ions and neutrals	E_{el}/H	E_{el+ZPE}/H	$\Delta E_{el+ZPE,0K}/\text{kJ mol}^{-1}$	$\Delta H_{298}/\text{kJ mol}^{-1}$	$\Delta G_{298}/\text{kJ mol}^{-1}$	$\Delta S_{298}/\text{J K}^{-1} \text{mol}^{-1}$
$[C_{15}H_{12}N]^+ + C_6H_{10}$	-867.860473	-867.481871	108.7	110.5	55.6	187.2
$[C_{15}H_{11}N]^+ + C_6H_{11}\cdot$	-867.762635	-867.388801	353.0	356.4	294.4	211.2
$[C_{15}H_{11}N]^+ + H\cdot + C_6H_{10}$	-867.700157	-867.335716	492.4	500.5	408.5	313.4
$[C_{14}H_{11}]^+ + HCN + C_6H_{10}$	-867.805171	-867.434369	233.4	239.5	134.6	357.4
$[C_{14}H_{11}]^+ + CNH + C_6H_{10}$	-867.767390	-867.398103	328.6	335.8	229.50	362.2

Table 4. Relative Energies of the Minima, Transition Structures, and Separated Products of Branched C_4H_9 Substituent (Tertiary-Butyl), $[C_{19}H_{20}N]^+$, Calculated at the M06-2X/6-311G(2d,2p) Level of Theory

Minima and TSs	E_{el}/H	E_{el+ZPE}/H	$\Delta E_{el+ZPE,0K}/kJ\ mol^{-1}$	$\Delta H_{298}/kJ\ mol^{-1}$	$\Delta G_{298}/kJ\ mol^{-1}$	$\Delta S_{298}/J\ K^{-1}\ mol^{-1}$
GM	-867.907197	-867.52326	0	0	0	0
2-Methylprop-1-ene loss TS	-790.410426	-790.074464	199.3	202.9	189.6	45.2
27 u loss proton transfer TS	-790.354477	-790.021697	337.9	339.5	286.0	182.3
Trans-cis rotation TS	-790.368795	-790.034717	303.7	306.9	248.6	198.9
HCN loss TS	-790.366286	-790.034831	303.4	306.7	250.5	191.7
Products ions and neutrals	E_{el}/H	E_{el+ZPE}/H	$\Delta E_{el+ZPE,0K}/kJ\ mol^{-1}$	$\Delta H_{298}/kJ\ mol^{-1}$	$\Delta G_{298}/kJ\ mol^{-1}$	$\Delta S_{298}/J\ K^{-1}\ mol^{-1}$
$[C_{15}H_{12}N]^++C_4H_8$	-790.448096	-790.107235	133.3	113.3	60.8	178.9
$[C_{14}H_{11}]^++HCN+C_4H_8$	-790.392740	-790.060231	236.7	242.8	139.6	351.7
$[C_{14}H_{11}]^++CNH+C_4H_8$	-790.354959	-790.023965	331.9	339.1	234.5	356.5

GM is the global minimum of the potential energy surface of the branched substituent C_4H_9

process of isomerization, followed by dissociation (Scheme 2b). Our electronic structure calculations indicate that a small energetic preference (8–14 $kJ\ mol^{-1}$) exists for the more complex process in which the rate-determining step is isomerization of the linear alkyl side chain to form a branched intermediate (Figure 4; Figures S6 and S7; Tables 2, S1–S3). This mechanism is consistent with the deuterated, $[M+D]^+$, spectra (Figure S1; Scheme S1). Additionally, we performed RRKM calculations to provide a better understanding of the relative competitiveness of these two pathways as a function of energy and time (Figure S8). The RRKM calculations indicate that the rate-determining step is always isomerization, prior to dissociation, and that the larger alkyl chains generally had lower rate constants than did the shorter ones. This result is much more consistent with our $E_{50\%}$ values than the degree of freedom scaled ones.

This rearrangement process involved both a 1,2-H-shift and a 1,2-N-shift, and required at least 263–270 $kJ\ mol^{-1}$ to initiate (Scheme 2; Figure 4a; Figure S6 and S7; Tables 2, S1–S3), depending on alkyl chain length. Dissociation of the branched intermediate formed occurred by a concerted mechanism where the C–N bond cleavage and proton abstraction accompany alkene formation (227–235 $kJ\ mol^{-1}$). The competing, more direct process (Scheme 2a; Figure 4b, Figure S9) essentially involved this same reaction type but produced higher energy transition structures (277–279 $kJ\ mol^{-1}$) due to the reduced charge stabilization of the transition structure available from the linear substituents. This discovery prompted the logical examination of branched systems to test whether this lowering of dissociation threshold in branched systems was general.

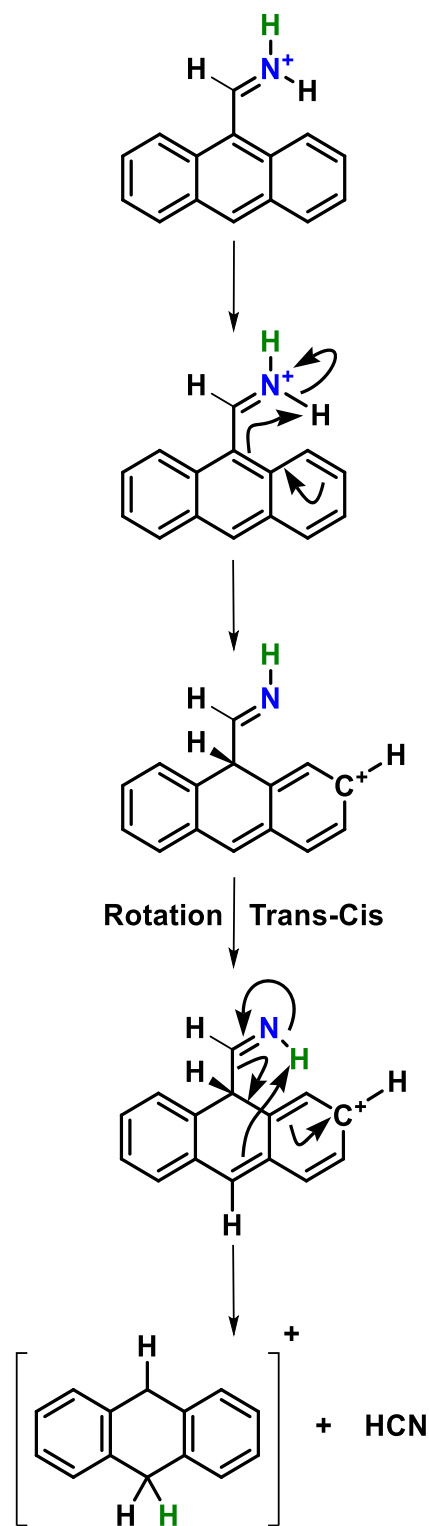
The branched analytes have no need to isomerize prior to cleaving the alkyl side chain. Consistent with this and the experimental data, our calculations predict that less energy was necessary to initiate fragmentation of the cyclohexyl and tertiary-butyl forms than the analytes with linear alkyl chains. Generation and expulsion of cyclohexene and 2-methylprop-1-ene, respectively, from these systems occurs via similar mechanisms (Scheme 3). The rate-limiting cyclohexene expulsion transition structure required at least 234 $kJ\ mol^{-1}$ (Figure 5a, Figure S10;

Table 3) whereas the 2-methylprop-1-ene expulsion required at least 199 $kJ\ mol^{-1}$ to initiate (Figure 5b, Figure S11; Table 4). These barriers are distinct from the linear forms and each other reflecting the systematic stabilization of the rate-limiting transition structures in the increasingly branched analyte ions. The deuterated data (Figures S2 and S3; Scheme S2) and RRKM calculations (Figure S12) are consistent with these mechanisms too.

Mechanisms of Consecutive Loss of 27 u (HCN or NCH Loss)

Each of the model system investigated here generates the anthracen-9-ylmethaniminium ion, $[C_{15}H_{12}N]^+$, detected at m/z 206. This ion expels a 27 u fragment (HCN or CNH) to form the abundant m/z 179, $[C_{14}H_{11}]^+$ peak (Figure S4, Figures 1, 2, and 3). A simple, direct mechanism for this dissociation was not immediately clear. Our calculations (Scheme 4; Figure 6; Tables 2, 3, and 4 and S1–S3) support a HCN loss lowest energy pathway in a multistep process beginning with rate-limiting proton (deuteron) transfer from the protonated imine nitrogen to carbon 9 of the ring. This transfer requires at least 328–338 $kJ\ mol^{-1}$ in order to occur (depending on from which precursor the anthracen-9-ylmethaniminium ion was generated) and triggers delocalization of the positive charge over the ring (Figure 6a, Figure S13). Note that a formal positive charge has been drawn on the right-hand side of the anthracene ring in Scheme 4 for the purpose of mechanistic illustration. Overcoming a subsequent, trans-cis rotational barrier (294–304 $kJ\ mol^{-1}$) places the remaining imine nitrogen proton in position for concerted transfer to carbon 10 on the anthracene ring and loss of HCN (TSs 294–303 $kJ\ mol^{-1}$; Scheme 4; Figure 6a, Figure S13). This mechanism is entirely consistent with the $[M+D]^+$ data (Figures S1–S3; Schemes S1–S3).

The alternate loss of the higher energy isomer CNH (55 $kJ\ mol^{-1}$) was also investigated. This process (Figure 6b) begins identically to the mechanism of loss of HCN and thus shares several structures (blue line, Figure 6b). Subsequent cleavage (red line, Figure 6b) of the imine to anthracene C–C bond in a twisting motion forms a proton bound dimer in which the formerly Ca hydrogen of the imine group is left pointing at C1 of the



Scheme 4. Schematic representation of the mechanism of HCN loss from anthracen-9-ylmethaniminium ion, forming $[C_{14}H_{11}]^+$, m/z 179. This reaction requires trans-cis rotation of the imine proton to facilitate HCN loss. Note that the calculations predict that the charge is delocalized in the final product.

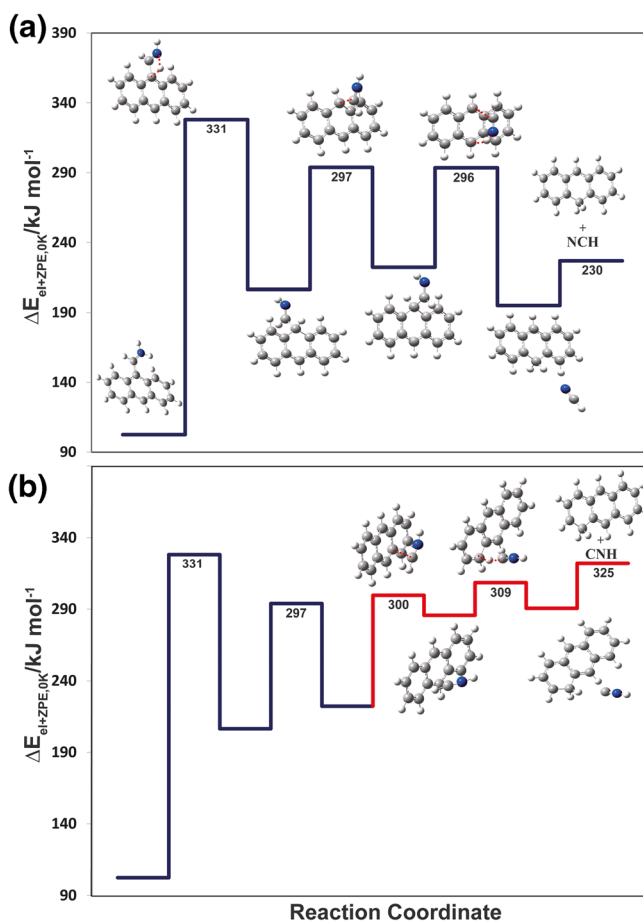


Figure 6. Minimum energy reaction pathway plots for anthracen-9-ylmethaniminium ion degradation. (a) Loss of HCN to form $[C_{14}H_{11}]^+$, m/z 179. (b) Loss of CNH to form an alternate $[C_{14}H_{11}]^+$ isomer, m/z 179. The red line indicates where the two pathways differ. Values of the TSs and separated products are provided for clarity (kJ mol^{-1})

anthracene ring. Abstraction of this proton produces another dimer which then dissociates to yield anthracene protonated at C1 and CNH. This entire pathway is limited by the initial proton (deuteron) transfer transition structure to the ring, just like the HCN loss pathway so both product types are possible. This initial proton transfer is highly energetically demanding and thus rate-limiting as it removes the conjugation from the central anthracene ring. Again, the mechanism is entirely consistent with the $[M+D]^+$ data (Figures S1–S3; Schemes S1–S3).

Other Fragmentation Processes

At higher collision energies, radical cations were detected from the precursor ions with linear alkyl substituents, and to a much smaller degree from the precursor ions with branched substituents. Consistent with experiment, where available, direct formation of these ions is predicted to be enthalpically unfavorable ($\geq 354 \text{ kJ mol}^{-1}$; Tables 2, 3, and 4 and S1–S3) compared with the closed-shell alkene losses ($\leq 270 \text{ kJ mol}^{-1}$). These pathways have higher but more similar thresholds to the

pathways for closed-shell, consecutive loss of HCN or CNH, but are massively entropically disfavored ($\Delta S_{298\text{ K}} = 17\text{--}29\text{ J K}^{-1}\text{ mol}^{-1}$ versus $> 170\text{ J K}^{-1}\text{ mol}^{-1}$) as they are competing with consecutive processes. Alternate, consecutive formation processes to generate radical cation species are significantly enthalpically unfavorable too ($> 500\text{ kJ mol}^{-1}$). Consequently, none of these processes were investigated further.

Conclusion

Our combined experimental and computational evidence indicates that the degree of branching of alkyl substituents is the key determining factor in their relative ease of dissociation (linear < secondary < tertiary). The lowest energy degradation pathways were common across compounds and involved loss of the branched alkyl substituent as an alkene. Linear substituents preferentially isomerized to branched forms prior to this loss. The chemistry underlying these related processes is dominated by the ability to stabilize the rate-determining transition structures, a task more effectively undertaken by branched substituents. The m/z 206 anthracen-9-ylmethaniminium ion generated from these alkene loss reactions undergoes rate-limiting proton transfer prior to expulsion of hydrogen cyanide or CNH. Proposed mechanisms were consistent with the deuterated analyte and pseudo-MS³ experimental findings. The combination of the differences in primary fragmentation thresholds and degree of radical-based fragmentation processes provide a potential means of distinguishing compounds that contain branched alkyl chain substituents from those with linear ones.

In subsequent work, we will expand these investigations to encompass a wider suite of analytes with a more diverse range of substituents and also modes of ionization. This will enable a broader understanding of $C_6H_7N_1$ series including other functional groups (e.g., acridinic and pyrrolic nitrogen derivatives, and other amines), isomeric species, and the variation in their tandem mass spectra and fragmentation energetics.

Acknowledgements

This work was supported by an American Chemical Society Petroleum Research Fund grant (56678-DNI6) and a University of Missouri Research Board Award. Maha T. Abutokaikah thanks the Saudi Arabia Culture Mission for funding part of her graduate work and the University of Missouri St. Louis for a Graduate Fellowship. Calculations were performed at the University of Missouri Science and Technology Rolla, MO.

References

1. Marshall, A.G., Rodgers, R.P.: Petroleomics: the next grand challenge for chemical analysis. *Acc. Chem. Res.* **37**, 53–59 (2004)
2. Marshall, A.G., Rodgers, R.P.: Petroleomics: chemistry of the underworld. *Proc. Natl. Acad. Sci.* **105**, 18090–18095 (2008)
3. Smith, D.F., Klein, G.C., Yen, A.T., Squicciarini, M.P., Rodgers, R.P., Marshall, A.G.: Crude oil polar chemical composition derived from FT

- ICR mass spectrometry accounts for asphaltene inhibitor specificity. *Energy Fuel.* **22**, 3112–3117 (2008)
4. Rodgers, R.P., McKenna, A.M.: Petroleum analysis. *Anal. Chem.* **83**, 4665–4687 (2011)
 5. Hsu, C.S., Hendrickson, C.L., Rodgers, R.P., McKenna, A.M., Marshall, A.G.: Petroleomics: advanced molecular probe for petroleum heavy ends. *J. Mass Spectrom.* **46**, 337–343 (2011)
 6. Savory, J.J., Kaiser, N.K., McKenna, A.M., Xian, F., Blakney, G.T., Rodgers, R.P., Hendrickson, C.L., Marshall, A.G.: Parts-per-billion Fourier transform ion cyclotron resonance mass measurement accuracy with a “walking” calibration equation. *Anal. Chem.* **83**, 1732–1736 (2011)
 7. Kind, T., Fiehn, O.: Seven Golden Rules for heuristic filtering of molecular formulas obtained by accurate mass spectrometry. *BMC Bioinf.* **8**, 105 (2007)
 8. McLafferty, F.W.: Tandem mass spectrometry. *Science.* **214**, 280–287 (1981)
 9. Bythell, B.J.: Comment on: “Quantum chemical mass spectrometry: verification and extension of the mobile proton model for histidine” by Julie Cautereels and Frank Blockhuys, *J. Am. Soc. Mass Spectrom.* **28**, 1227–1235 (2017). *J. Am. Soc. Mass Spectrom.* **28**, 2728–2730 (2017)
 10. Domokos, L., Hennberg, D., Weimann, B.: Computer-aided identification of compounds by comparison of mass spectra. *Anal. Chim. Acta.* **165**, 61–74 (1984)
 11. NIST/EPA/NIH Mass Spectral Library: NIST Version 17, <https://www.nist.gov/srd/nist-standard-reference-database-1a-v17>
 12. Eng, J.K., McCormack, A.L., Yates, J.R.: An approach to correlate tandem mass spectral data of peptides with amino acid sequences in a protein database. *J. Am. Soc. Mass Spectrom.* **5**, 976–989 (1994)
 13. Perkins, D.N., Pappin, D.J., Creasy, D.M., Cottrell, J.S.: Probability-based protein identification by searching sequence databases using mass spectrometry data. *Electrophoresis.* **20**, 3551–3567 (1999)
 14. Frank, A., Pevzner, P.: PepNovo: de novo peptide sequencing via probabilistic network modeling. *Anal. Chem.* **77**, 964–973 (2005)
 15. Frewen, B.E., Merrihew, G.E., Wu, C.C., Noble, W.S., MacCoss, M.J.: Analysis of peptide MS/MS spectra from large-scale proteomics experiments using spectrum libraries. *Anal. Chem.* **78**, 5678–5684 (2006)
 16. Nesvizhskii, A.I.: Protein identification by tandem mass spectrometry and sequence database searching. *Methods Mol. Biol.* **367**, 87–119 (2007)
 17. Lam, H., Aebersold, R.: Building and searching tandem mass (MS/MS) spectral libraries for peptide identification in proteomics. *Methods.* **54**, 424–431 (2011)
 18. Podgorski, D.C., Corilo, Y.E., Nyadong, L., Lobodin, V.V., Bythell, B.J., Robbins, W.K., McKenna, A.M., Marshall, A.G., Rodgers, R.P.: Heavy petroleum composition. 5. Compositional and structural continuum of petroleum revealed. *Energy Fuel.* **27**, 1268–1276 (2013)
 19. Qian, K., Edwards, K.E., Mennito, A.S., Freund, H., Saeger, R.B., Hickey, K.J., Francisco, M.A., Yung, C., Chawla, B., Wu, C., Kushnerick, J.D., Olmstead, W.N.: Determination of structural building blocks in heavy petroleum systems by collision-induced dissociation Fourier transform ion cyclotron resonance mass spectrometry. *Anal. Chem.* **84**, 4544–4551 (2012)
 20. Fernandez-Lima, F.A., Becker, C., McKenna, A.M., Rodgers, R.P., Marshall, A.G., Russell, D.H.: Petroleum crude oil characterization by IMS-MS and FTICR MS. *Anal. Chem.* **81**, 9941–9947 (2009)
 21. Kim, S., Rodgers, R.P., Blakney, G.T., Hendrickson, C.L., Marshall, A.G.: Automated electrospray ionization FT-ICR mass spectrometry for petroleum analysis. *J. Am. Soc. Mass Spectrom.* **20**, 263–268 (2009)
 22. Shi, Q., Hou, D., Chung, K.H., Xu, C., Zhao, S., Zhang, Y.: Characterization of heteroatom compounds in a crude oil and its saturates, aromatics, resins, and asphaltenes (SARA) and non-basic nitrogen fractions analyzed by negative-ion electrospray ionization Fourier transform ion cyclotron resonance mass spectrometry. *Energy Fuel.* **24**, 2545–2553 (2010)
 23. Hughey, C.A., Rodgers, R.P., Marshall, A.G.: Resolution of 11 000 compositionally distinct components in a single electrospray ionization Fourier transform ion cyclotron resonance mass spectrum of crude oil. *Anal. Chem.* **74**, 4145–4149 (2002)
 24. Qian, K., Robbins, W.K., Hughey, C.A., Cooper, H.J., Rodgers, R.P., Marshall, A.G.: Resolution and identification of elemental compositions for more than 3000 crude acids in heavy petroleum by negative-ion microelectrospray high-field Fourier transform ion cyclotron resonance mass spectrometry. *Energy Fuel.* **15**, 1505–1511 (2001)
 25. Rodgers, R.P., Marshall, A.G.: Petroleomics: advanced characterization of petroleum-derived materials by Fourier transform ion cyclotron

- resonance mass spectrometry (FT-ICR MS). In: *Asphaltenes, heavy oils, and petroleomics*. pp. 63–93 (2007)
26. Klein, G.C., Kim, S., Rodgers, R.P., Marshall, A.G., Yen, A.: Mass spectral analysis of asphaltenes. II. Detailed compositional comparison of asphaltenes deposit to its crude oil counterpart for two geographically different crude oils by ESI FT-ICR MS. *Energy Fuel*. **20**, 1973–1979 (2006)
27. McKenna, A.M., Purcell, J.M., Rodgers, R.P., Marshall, A.G.: Heavy petroleum composition. I. Exhaustive compositional analysis of Athabasca bitumen HVGO distillates by Fourier transform ion cyclotron resonance mass spectrometry: a definitive test of the Boduszynski model. *Energy Fuel*. **24**, 2929–2938 (2010)
28. Corilo, Y.E., Vaz, B.G., Simas, R.C., Lopes Nascimento, H.D., Klitzke, C.F., Pereira, R.C.L., Bastos, W.L., Santos Neto, E.V., Rodgers, R.P., Eberlin, M.N.: *Petroleomics by EASI(±) FT-ICR MS*. *Anal. Chem.* **82**, 3990–3996 (2010)
29. McKenna, A.M., Donald, L.J., Fitzsimmons, J.E., Juyal, P., Spicer, V., Standing, K.G., Marshall, A.G., Rodgers, R.P.: Heavy petroleum composition. 3. Asphaltene aggregation. *Energy Fuel*. **27**, 1246–1256 (2013)
30. Purcell, J.M., Rodgers, R.P., Hendrickson, C.L., Marshall, A.G.: Speciation of nitrogen containing aromatics by atmospheric pressure photoionization or electrospray ionization Fourier transform ion cyclotron resonance mass spectrometry. *J. Am. Soc. Mass Spectrom.* **18**, 1265–1273 (2007)
31. Schaub, T.M., Rodgers, R.P., Marshall, A.G., Qian, K., Green, L.A., Olmstead, W.N.: Speciation of aromatic compounds in petroleum refinery streams by continuous flow field desorption ionization FT-ICR mass spectrometry. *Energy Fuel*. **19**, 1566–1573 (2005)
32. Wittrig, A.M., Fredriksen, T.R., Qian, K., Clingenpeel, A.C., Harper, M.R.: Single Dalton collision-induced dissociation for petroleum structure characterization. *Energy Fuel*. **31**, 13338–13344 (2017)
33. Rodgers, R.P., Schaub, T.M., Marshall, A.G.: *Petroleomics: MS returns to its roots*. *Anal. Chem.* **77**, 20 A–27 A (2005)
34. Ruddy, B.M., Huettel, M., Kostka, J.E., Lobodin, V.V., Bythell, B.J., McKenna, A.M., Aeppli, C., Reddy, C.M., Nelson, R.K., Marshall, A.G., Rodgers, R.P.: Targeted petroleomics: analytical investigation of Macondo well oil oxidation products from Pensacola Beach. *Energy Fuel*. **28**, 4043–4050 (2014)
35. Atlas, R.M.: Fate of oil from two major oil spills: role of microbial degradation in removing oil from the Amoco Cadiz and IXTOC I spills. *Environ. Int.* **5**, 33–38 (1981)
36. Aeppli, C., Carmichael, C.A., Nelson, R.K., Lemkau, K.L., Graham, W.M., Redmond, M.C., Valentine, D.L., Reddy, C.M.: Oil weathering after the Deepwater Horizon disaster led to the formation of oxygenated residues. *Environ. Sci. Technol.* **46**, 8799–8807 (2012)
37. Short, J.W., Irvine, G.V., Mann, D.H., Masekko, J.M., Pella, J.J., Lindeberg, M.R., Payne, J.R., Driskell, W.B., Rice, S.D.: Slightly weathered Exxon Valdez oil persists in Gulf of Alaska beach sediments after 16 years. *Environ. Sci. Technol.* **41**, 1245–1250 (2007)
38. Stenson, A.C., Marshall, A.G., Cooper, W.T.: Exact masses and chemical formulas of individual Suwannee River fulvic acids from ultrahigh resolution electrospray ionization Fourier transform ion cyclotron resonance mass spectra. *Anal. Chem.* **75**, 1275–1284 (2003)
39. Stenson, A.C., Landing, W.M., Marshall, A.G., Cooper, W.T.: Ionization and fragmentation of humic substances in electrospray ionization Fourier transform-ion cyclotron resonance mass spectrometry. *Anal. Chem.* **74**, 4397–4409 (2002)
40. Stenson, A.C., Ruddy, B.M., Bythell, B.J.: Ion molecule reaction H/D exchange as a probe for isomeric fractionation in chromatographically separated natural organic matter. *Int. J. Mass Spectrom.* **360**, 45–53 (2014)
41. Brown, T.A., Jackson, B.A., Bythell, B.J., Stenson, A.C.: Benefits of multidimensional fractionation for the study and characterization of natural organic matter. *J. Chromatogr. A*. **1470**, 84–96 (2016)
42. Bai, H., Jiang, W., Kotchey, G.P., Saidi, W.A., Bythell, B.J., Jarvis, J.M., Marshall, A.G., Robinson, R.A.S., Star, A.: Insight into the mechanism of graphene oxide degradation via the photo-Fenton reaction. *J. Phys. Chem. C*. **118**, 10519–10529 (2014)
43. West, B., Sit, A., Mohamed, S., Joblin, C., Blanchet, V., Bodi, A., Mayer, P.M.: Dissociation of the anthracene radical cation: a comparative look at iPEPICO and collision-induced dissociation mass spectrometry results. *J. Phys. Chem. A*. **118**, 9870–9878 (2014)
44. Mayer, P.M., Blanchet, V., Joblin, C.: Threshold photoelectron study of naphthalene, anthracene, pyrene, 1,2-dihydronaphthalene, and 9,10-dihydroanthracene. *J. Chem. Phys.* **134**, 244312 (2011)
45. Johansson, H.A.B., Zettergren, H., Holm, A.I.S., Haag, N., Nielsen, S.B., Wyer, J.A., Kirketerp, M.-B.S., Stöckel, K., Hvelplund, P., Schmidt, H.T., Cederquist, H.: Unimolecular dissociation of anthracene and acridine cations: the importance of isomerization barriers for the C2H2 loss and HCN loss channels. *J. Chem. Phys.* **135**, 084304 (2011). <https://doi.org/10.1063/1.3626792>
46. Jarrell, T.M., Jin, C., Riedeman, J.S., Owen, B.C., Tan, X., Scherer, A., Tykwinski, R.R., Gray, M.R., Slater, P., Kenttämä, H.I.: Elucidation of structural information achievable for asphaltenes via collision-activated dissociation of their molecular ions in MSⁿ experiments: a model compound study. *Fuel*. **133**, 106–114 (2014)
47. Borton, D., Pinkston, D.S., Hurt, M.R., Tan, X., Azyat, K., Scherer, A., Tykwinski, R., Gray, M., Qian, K., Kenttämä, H.I.: Molecular structures of asphaltenes based on the dissociation reactions of their ions in mass spectrometry. *Energy Fuel*. **24**, 5548–5559 (2010)
48. Oomens, J., Sartakov, B.G., Meijer, G., von Helden, G.: Gas-phase infrared multiple photon dissociation spectroscopy of mass-selected molecular ions. *Int. J. Mass Spectrom.* **254**, 1–19 (2006)
49. Oomens, J., Tielens, A.G.G.M., Sartakov, B.G., von Helden, G., Meijer, G.: Laboratory infrared spectroscopy of cationic polycyclic aromatic hydrocarbon molecules. *Astrophys. J.* **591**, 968–985 (2003)
50. Oomens, J., van Rooij, A.J.A., Meijer, G., von Helden, G.: Gas-phase infrared photodissociation spectroscopy of cationic polyaromatic hydrocarbons. *Astrophys. J.* **542**, 404–410 (2000)
51. Oomens, J., Meijer, G., von Helden, G.: Gas phase infrared spectroscopy of cationic indane, acenaphthene, fluorene, and fluoranthene. *J. Phys. Chem. A*. **105**, 8302–8309 (2001)
52. Carpenter, J.E., McNary, C.P., Furin, A., Sweeney, A.F., Armentrout, P.B.: How hot are your ions really? A threshold collision-induced dissociation study of substituted benzylpyridinium “thermometer” ions. *J. Am. Soc. Mass Spectrom.* **28**, 1876–1888 (2017)
53. Zins, E.-L., Pepe, C., Schröder, D.: Energy-dependent dissociation of benzylpyridinium ions in an ion-trap mass spectrometer. *J. Mass Spectrom.* **45**, 1253–1260 (2010)
54. Morsa, D., Gabelica, V., Rosu, F., Oomens, J., De Pauw, E.: Dissociation pathways of benzylpyridinium “thermometer” ions depend on the activation regime: an IRMPD spectroscopy study. *J. Phys. Chem. Lett.* **5**, 3787–3791 (2014)
55. Gatineau, D., Memboeuf, A., Milet, A., Cole, R.B., Dossmann, H., Gimbert, Y., Lesage, D.: Experimental bond dissociation energies of benzylpyridinium thermometer ions determined by threshold-CID and RRKM modeling. *Int. J. Mass Spectrom.* **417**, 69–75 (2017)
56. Milasinovic, S., Cui, Y., Gordon, R.J., Hanley, L.: Internal energy of thermometer ions formed by femtosecond laser desorption: implications for mass spectrometric imaging. *J. Phys. Chem. C*. **118**, 28938–28947 (2014)
57. Barylyuk, K.V., Chingin, K., Balabin, R.M., Zenobi, R.: Fragmentation of benzylpyridinium “thermometer” ions and its effect on the accuracy of internal energy calibration. *J. Am. Soc. Mass Spectrom.* **21**, 172–177 (2010)
58. Derwa, F., de Pauw, E., Natalis, P.: New basis for a method for the estimation of secondary ion internal energy distribution in ‘soft’ ionization techniques. *Org. Mass Spectrom.* **26**, 117–118 (1991)
59. Flanigan, P.M., Shi, F., Perez, J.J., Karki, S., Pfeiffer, C., Schafmeister, C., Levis, R.J.: Determination of internal energy distributions of laser electrospray mass spectrometry using thermometer ions and other biomolecules. *J. Am. Soc. Mass Spectrom.* **25**, 1572–1582 (2014)
60. Greisch, J.-F., Gabelica, V., Remacle, F., Pauw, E.D.: Thermometer ions for matrix-enhanced laser desorption/ionization internal energy calibration. *Rapid Commun. Mass Spectrom.* **17**, 1847–1854 (2003)
61. Collette, C., Drahos, L., Pauw, E.D., Vékey, K.: Comparison of the internal energy distributions of ions produced by different electrospray sources. *Rapid Commun. Mass Spectrom.* **12**, 1673–1678 (1998)
62. Gabelica, V., Pauw, E.D.: Internal energy and fragmentation of ions produced in electrospray sources. *Mass Spectrom. Rev.* **24**, 566–587 (2005)
63. Vala, M., Oomens, J., Berden, G.: Structure and dissociation pathways of protonated tetralin (1,2,3,4-tetrahydronaphthalene). *J. Phys. Chem. A*. **121**, 4606–4612 (2017)
64. Walker, S.W.C., Mark, A., Verbuyst, B., Bogdanov, B., Campbell, J.L., Hopkins, W.S.: Characterizing the tautomers of protonated aniline using

- differential mobility spectrometry and mass spectrometry. *J. Phys. Chem. A*. **122**, 3858–3865 (2018)
65. Bythell, B.J., Corilo, Y., Lobodin, V.V., Rodgers, R.P., Marshall, A.G.: Model Compound Fragmentation Pathways as an Entry to Structural Analysis of Crude Oil. American Society of Mass Spectrometry Conference, Minneapolis (2013)
66. Bythell, B.J., Corilo, Y., Jarvis, J.M., Lobodin, V.V., Rodgers, R.P., Marshall, A.G.: Analysis of Crude Oil MS/MS Fragmentation Patterns. 9th North American FT MS Conference, Key West, FL (2013)
67. Wilcke, W.: Global patterns of polycyclic aromatic hydrocarbons (PAHs) in soil. *Geoderma*. **141**, 157–166 (2007)
68. Culotta, L., Gianguzza, A., Mannino, M.R., Orecchio, S.: Polycyclic aromatic hydrocarbons (pah) in Vulcano Island (aeolian archipelago) mud utilized for therapeutic purpose. *Polycycl. Aromat. Compd.* **27**, 281–294 (2007)
69. Lima, A.L.C., Farrington, J.W., Reddy, C.M.: Combustion-derived polycyclic aromatic hydrocarbons in the environment—a review. *Environ. Forensic*. **6**, 109–131 (2005)
70. St-Amand, A.D., Mayer, P.M., Blais, J.M.: Modeling PAH uptake by vegetation from the air using field measurements. *Atmos. Environ.* **43**, 4283–4288 (2009)
71. Tielens, A.G.G.M.: Interstellar polycyclic aromatic hydrocarbon molecules. *Annu. Rev. Astron. Astrophys.* **46**, 289–337 (2008)
72. Tabet, J.C., Fraise, D.: Reaction of cyclohexanone with $[NH_4]^+$ under chemical ionization conditions. I—formation of protonated unsubstituted imines. *Org. Mass Spectrom.* **16**, 45–47 (1981)
73. Benassi, M., Garcia-Reyes, J.F., Spengler, B.: Ambient ion/molecule reactions in low-temperature plasmas (LTP): reactive LTP mass spectrometry. *Rapid Commun. Mass Spectrom.* **27**, 795–804 (2013)
74. Bythell, B.J., Maitre, P., Paizs, B.: Cyclization and rearrangement reactions of an fragment ions of protonated peptides. *J. Am. Chem. Soc.* **132**, 14766–14779 (2010)
75. Bythell, B.J., Hernandez, O., Steinmetz, V., Paizs, B., Maitre, P.: Tyrosine side-chain catalyzed proton transfer in the YG a2 ion revealed by theory and IR spectroscopy in the ‘fingerprint’ and XH (X=C, N, O) stretching regions. *Int. J. Mass Spectrom.* **316–318**, 227–234 (2012)
76. Paizs, B., Suhai, S.: Combined quantum chemical and RRKM modeling of the main fragmentation pathways of protonated GGG. I. Cis-trans isomerization around protonated amide bonds. *Rapid Commun. Mass Spectrom.* **15**, 2307–2323 (2001)
77. Kullman, M.J., Molesworth, S., Berden, G., Oomens, J., Van Stipdonk, M.: IRMPD spectroscopy b2 ions from protonated tripeptides with 4-aminomethyl benzoic acid residues. *Int. J. Mass Spectrom.* **316–318**, 174–181 (2012)
78. Zhao, J., Lau, J.K.-C., Grzetic, J., Verkerk, U.H., Oomens, J., Siu, K.W.M., Hopkinson, A.C.: Structures of an* ions derived from protonated pentaglycine and pentaalanine: results from IRMPD spectroscopy and DFT calculations. *J. Am. Soc. Mass Spectrom.* **24**, 1957–1968 (2013)
79. Butler, M., Siu, K.W.M., Hopkinson, A.C.: Transnitrosylation products of the dipeptide cysteinyl-cysteine: an examination by tandem mass spectrometry and density functional theory. *Phys. Chem. Chem. Phys.* **18**, 6047–6052 (2016)
80. Zhang, D., Gill, L.A., Cooks, R.G.: Deamination of protonated amines to yield protonated imines. *J. Am. Soc. Mass Spectrom.* **9**, 1146–1157 (1998)
81. Bythell, B.J., Csonka, I.P., Suhai, S., Barofsky, D.F., Paizs, B.: Gas-phase structure and fragmentation pathways of singly protonated peptides with N-terminal arginine. *J. Phys. Chem. B*. **114**, 15092–15105 (2010)
82. Bouchoux, G., Choret, N., Berruyer-Penaud, F., Flammang, R.: Thermochemistry and unimolecular reactivity of protonated α,ω -aminoalcohols in the gas phase. *Int. J. Mass Spectrom.* **217**, 195–230 (2002)
83. Abutokaikah, M.T., Guan, S., Bythell, B.J.: Stereochemical sequence ion selectivity: proline versus pipercolic-acid-containing protonated peptides. *J. Am. Soc. Mass Spectrom.* **28**, 182–189 (2017)
84. Nelson, C.R., Abutokaikah, M.T., Harrison, A.G., Bythell, B.J.: Proton mobility in b2 ion formation and fragmentation reactions of histidine-containing peptides. *J. Am. Soc. Mass Spectrom.* **27**, 487–497 (2016)
85. Abutokaikah, M., Frye, J., Stump, C., Gnawali, G., Spilling, C.D., Bythell, B.J.: Aromatic core formation and side chain losses from series of isomeric model compounds of petroleum: energetics and practical applications. American Society of Mass Spectrometry Conference, San Diego (2018)
86. Jarrahpour, A., Nazari, M., Jalbout, A.F.: Synthesis and physical characterization of 4-(anthracen-10-yl)-1-cyclohexyl-3-phenoxyazetid-2-one as a new trans 2-azetidone. *Molbank*. **2007**, M538 (2007)
87. Ghosh, K., Masanta, G., Chattopadhyay, A.P.: Anthracene labeled pyridine amides: a class of prototype PET sensors towards monocarboxylic acid. *J. Photochem. Photobiol. A Chem.* **203**, 40–49 (2009)
88. Frisch, M.J.: Gaussian 09, Revision C.01. Gaussian, Inc., Wallingford (2010)
89. Zhao, Y., Truhlar, D.G.: The M06 suite of density functionals for main group thermochemistry, thermochemical kinetics, noncovalent interactions, excited states, and transition elements: two new functionals and systematic testing of four M06-class functionals and 12 other functionals. *Theor. Chem. Accounts*. **120**, 215 (2006)